the manufacturer's instructions. We analysed the expression of five genes: *matrix metallopeptidase 2 (MMP-2)*, *matrix metallopeptidase 7 (MMP-7)*, *matrix metallopeptidase 9 (MMP-9)*, *TF*, and *GAPDH* as an internal control gene. For all of these genes, we used commercially available TaqMan primers and probe mixture (Applied Biosystems). The reporter dye at the 5′ end of the probe was FAM™, and the quencher dye at the 3′ end was minor groove binder (MGB). Real-time PCR was performed using precycling heat activation at 95 °C for 20 s, followed by 40 cycles of denaturation at 95 °C for 3 s, and annealing/extension at 62 °C for 30 s, in the Applied Biosystems 7500 Fast Real-Time PCR System. Relative quantification of the total RNA in each sample was conducted using the comparative Ct (threshold cycle) method. In this analysis, the formulas for the relative quantification of each of the genes were as follows: (dCT of each gene) = (Ct of each gene) – (Ct of *GAPDH*), and (Relative quantification of each gene) = $2^{-(\text{dCt of each gene})}$.

2.6. *TF ELISA assay*

TF protein was measured by IMUBIND® Tissue Factor ELISA Kit (American Diagnostica, Greenwich, CT, USA) in accordance with the manufacturer's instructions.

2.7. *Cell invasion assay*

BxPC3 mock and BxPC3 TFshRNA (2.5×10^4 cells diluted in 500 μL of serum-free DMEM) were added to the upper wells of a Transwell® 24-well insert coated with Matrigel™ (BD Biosciences) according to the manufacturer's instructions. DMEM with 10% FBS was added to the lower wells. Cells were incubated for 22 h in an atmosphere of 5% CO_2 at 37 °C. Cells in the top wells were removed using cotton swabs. Invaded cells were stained and counted in three different viewing fields. In addition, to avoid the effect of factor VIIa in FBS, 500 μL of cell suspension in serum-free high-glucose DMEM was added to the upper wells after they were deprived of serum for 2 h, and high-glucose DMEM supplied with 1% BSA and 0.5% FBS was poured into the lower wells. Factor VIIa and anti-TF antibodies were also added to the lower wells. At the end of 48 h incubation at 5% CO_2, 37 °C, the cells in the top wells were removed and invaded cells were counted. Every invasion assay was conducted two times each.

2.8. *Gelatin zymography*

SDS-gelatin zymography was performed with 10% zymogram gel (Invitrogen). Cells (2×10^5) were seeded on a 6-well plate and incubated for 24 h at 37 °C. The medium was removed and incubated for 24 h in serum-free DMEM, after which the medium was collected. Tris–Glycine SDS Sample Buffer (Invitrogen) was added and incubated for 30 min at 37 °C. After electrophoresis at 4 °C, the gel was shaken with zymogram renaturing buffer for 30 min. Next, the zymogram renaturing buffer was removed and zymogram developing buffer (Invitrogen) was added and shaken for 30 min. The gel was added to new zymogram developing buffer and was incubated for 30 h at 37 °C. The gel was fixed and then stained with Quick CBB (Wako Chemicals). MMPs were quantified using Image J software.

2.9. *Effect of anti-TF mAb on invasion and metastasis in nude mice*

To assess metastasis and invasion, we established an orthotopic pancreatic cancer mouse model as described previously.[19] Briefly, BxPC3 mock or BxPC3 TFshRNA expressing GFP (5×10^6 cells) was injected into the body of the pancreas of nude mice after laparotomy under anaesthesia. The mice were sacrificed 5 weeks after the injection of cancer cells. An OV110 fluorescence microscope (Olympus, Tokyo, Japan) was used to observe several organs and a dissemination score was calculated to evaluate local tumour invasion and distant metastasis as previously described.[20] Tumour dissemination was quantified as follows: every manifestation of tumour infiltration or metastasis was credited with one point. Additional points were awarded for massive local infiltration, multiple metastatic nodules and metastatic nodules >50 mm^3. In treatment experiments, mice inoculated with $BxPC3^{Luc}$ or BxPC3 mock expressing GFP cells on Day 0 were treated for seven consecutive days with 1849 mAb (400 μg/mouse) as a TF neutralisation antibody, or PBS as a control. The IVIS imaging system (Caliper Life Sciences, Hopkinton, MA, USA) was used to observe tumour invasion of mice inoculated with $BxPC3^{Luc}$. After 40 days, mice inoculated with cells expressing GFP were sacrificed. A dissemination score was calculated. To assess the inhibition of haematogenous metastasis by anti-TF antibody, we established a portal-injection liver metastasis model. BxPC3 cells expressing luciferase (5×10^5 cells) were directly injected into the portal vein after intravenous administration of 1849 mAb (500 μg/mouse) or PBS as a control. The IVIS imaging system was used to detect liver micrometastasis. All animal experiments were performed in compliance with the Guidelines for the Care and Use of Experimental Animals established by the Committee for Animal Experimentation of the National Cancer Center, Japan; these guidelines meet the ethical standards required by law for proper conduct of animal experiments in Japan.

2.10. *Statistical analysis*

Student's *t*-test was used for the statistical analyses unless otherwise mentioned. $P < 0.05$ was considered significant.

3. Results

3.1. *TF-positive human pancreatic cancer cells, BxPC3, enhance invasion potential in vitro and in vivo*

We used the BxPC3 cell line in a series of our experiments because real-time PCR analysis and immunostaining of TF showed that BxPC3 strongly expressed TF amongst the four pancreatic cancer cell lines (Fig. 1A). Then, we examined the status of TF expression for BxPC3 *in vitro* and *in vivo*. Immunostaining revealed TF expression specifically in cancer cells contacting with stromal tissues, namely the invasive front *in vivo*, although TF expression was uniformly observed in all cells *in vitro* (Fig. 1B). To determine if TF affects pancreatic cancer invasion, we established TF-knockdown BxPC3 cell lines. BxPC3 cells were infected with TF shRNA lentivirus (BxPC3 TFshRNA) and non-target shRNA lentivirus (BxPC3

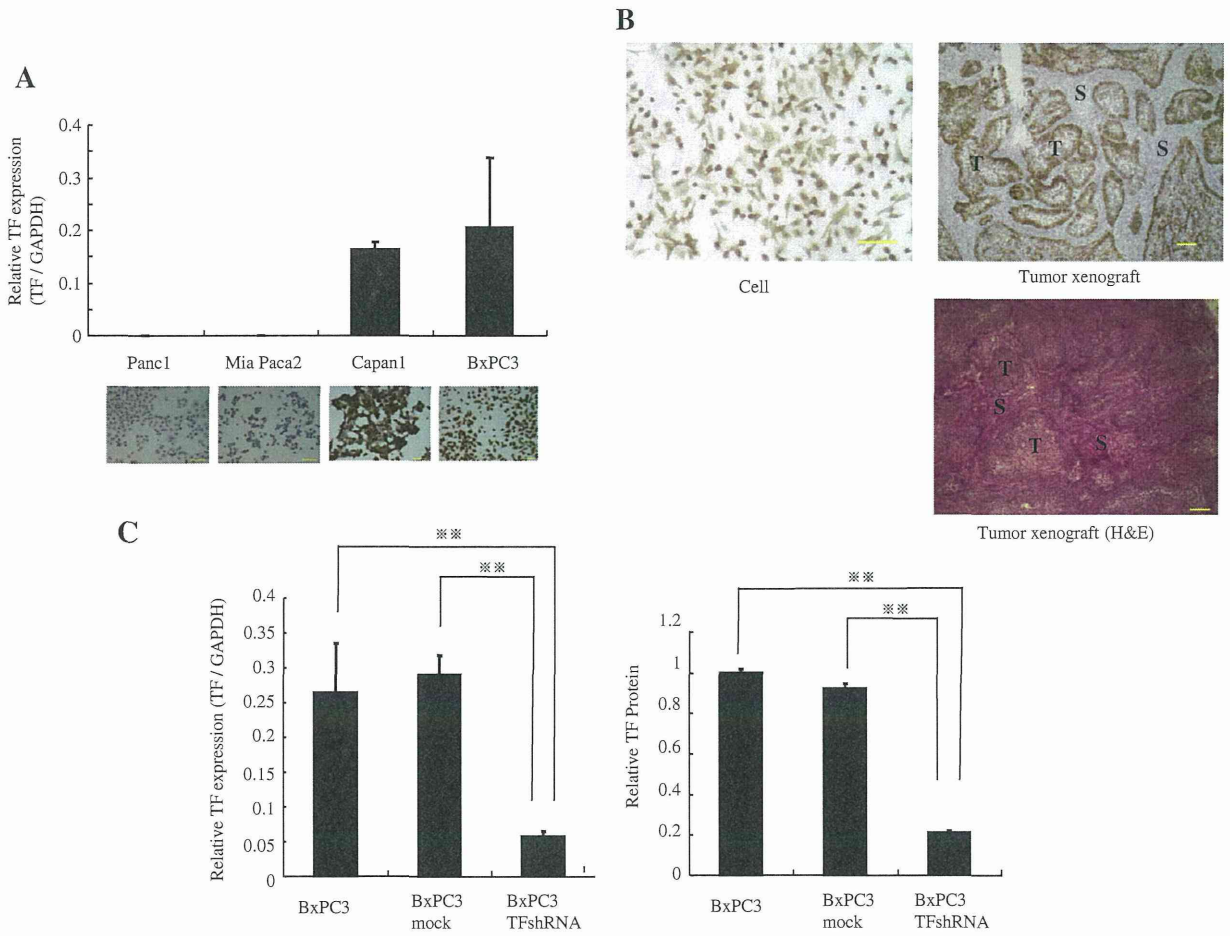

Fig. 1 – TF knockdown cells decrease the invasion ability. (A) Expression of TF amongst the four human pancreatic cancer cell lines *in vitro*. Total RNA was isolated and mRNA was quantitated by real-time PCR. Data are expressed as the mean ± SD. *N* = 3–4. The images show the staining of TF. Scale bar 100 μm. (B) Pattern of expression of TF in cultured cells and tumour xenografts. Scale bar 100 μm. T and S mean 'tumour' and 'stroma', respectively. (C) mRNA and protein level of TF in BxPC3, BxPC3 mock and BxPC3 TFshRNA. mRNA was quantitated by real-time PCR and TF protein was quantitated by TF ELISA. Data are expressed as the mean ± SD. *N* = 3–4. ** $P < 0.01$. (D) Invasion ability in BxPC3 mock and BxPC3 TFshRNA. BxPC3 mock and BxPC3 TFshRNA diluted in 500 μL of serum-free DMEM were added to the upper wells of a Transwell™ 24-well insert coated with Matrigel®. DMEM supplied with 10% FBS was added to the lower wells. Data are expressed as the mean ± SD. * $P < 0.05$. The images show the invasion cells. Scale bar 100 μm. (E) Representative fluorescence images of liver, mesentery, and stomach bearing BxPC3 mock GFP or BxPC3 TFshRNA GFP orthotopically. GFP signal denotes the presence of tumour cells. (F) A dissemination score was calculated to evaluate local tumour invasion and distant metastasis as previously described. Data are expressed as the mean ± SD. *N* = 4–6. ** $P < 0.01$.

mock) as a control. BxPC3 TFshRNA appeared to reduce TF expression by 80% at both the mRNA level and protein level (Fig. 1C). BxPC3 TFshRNA showed significant reduction in invasive ability compared with BxPC3 mock in DMEM medium containing 10% FBS (Fig. 1D). We next examined if TF promotes BxPC3 metastasis and invasion in the pancreatic orthotopic tumour xenografts. In the BxPC3 mock orthotopic tumour model, extensive invasion and metastasis was observed in the liver, mesentery and stomach (Fig. 1E). On the other hand, invasion and metastasis was suppressed in the BxPC3 TFshRNA orthotopic tumour model (Fig. 1E). The progression score reflecting tumour invasion and metastasis was significantly decreased in the BxPC3 TFshRNA tumour compared with the BxPC3 mock tumour (Fig 1F).

3.2. *TF-VIIa complex induces MMP-9 expression and promotes cancer cell invasion*

To determine a possible TF-mediated invasion factor in the BxPC3 cell line, we examined MMP-2, MMP-7 and MMP-9 expression levels by real-time PCR. Expression of MMP-2 and MMP-7 was very low both in BxPC3 mock and BxPC3 TFshRNA. In contrast, MMP-9 was highly expressed in BxPC3 mock and was significantly reduced in BxPC3 TFshRNA (Fig. 2A). We, therefore, clarified that TF induced MMP-9 production and promoted the invasion ability of pancreatic cancer cells under DMEM containing 10% FBS (Fig. 1). To avoid the effect of factor VIIa in FBS on MMP-9 expression and to determine whether or not the TF-VIIa complex induces MMP-9 followed by promoting

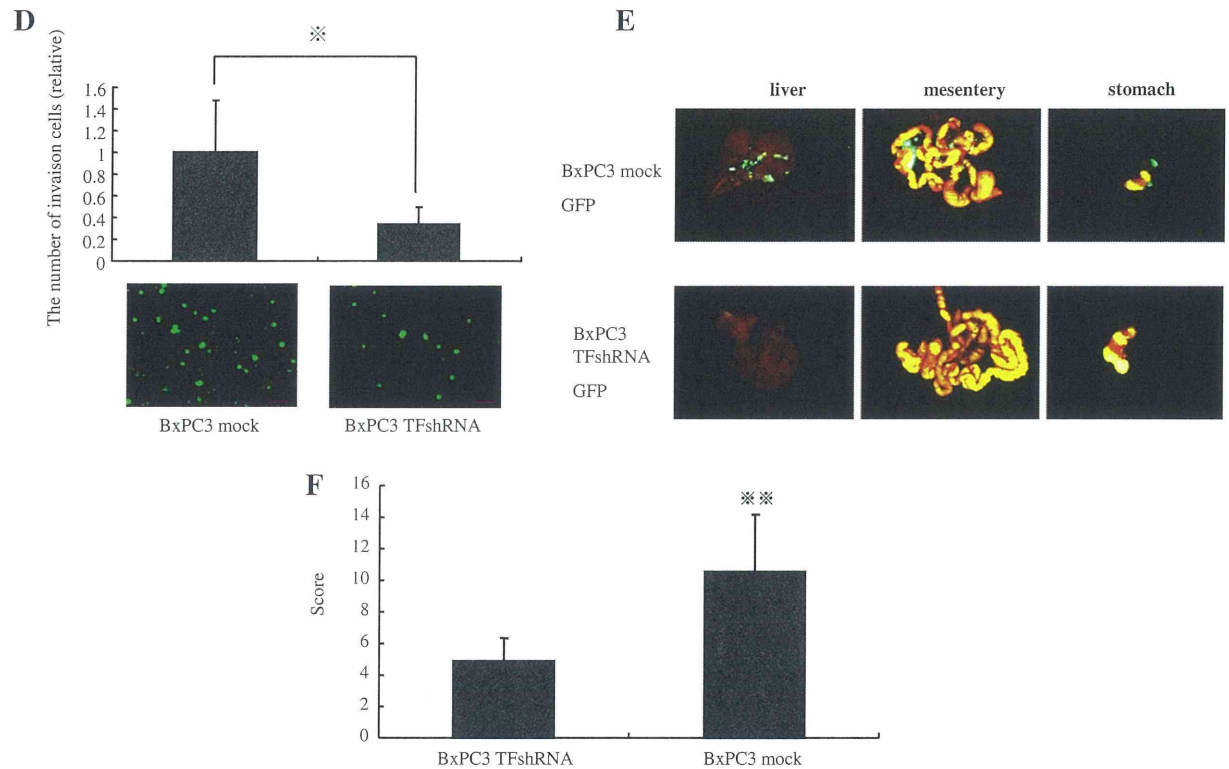

Fig 1. (*continued*)

BxPC3 cell invasion, BxPC3 was cultured under FBS-free DMEM (serum starvation). Gelatin zymography showed that BxPC3 mock with factor VIIa significantly increased MMP-9 production compared with BxPC3 mock without factor VIIa (Fig. 2B). However, MMP-9 was not detected in BxPC3 TFshRNA, with or without factor VIIa (Fig. 2B). Invasion assay showed that factor VIIa significantly enhanced the invasion ability of BxPC3 mock but not BxPC3 TFshRNA. This data strongly suggested that the TF-VIIa complex promotes MMP-9 production followed by enhancing cancer cell invasion (Fig. 2C).

3.3. *Establishment of neutralisation antibody that inhibits both the blood coagulation cascade and cell signalling of TF*

To establish an anti-human TF neutralisation antibody, we screened 14 hybridoma clones producing rat anti-human TF antibody. The supernatant of hybridoma clones 444 and 1849 significantly inhibited factor X activity (Supplemental Fig. A). Next, we purified the antibody from clones 1849, 72 and 130. The inhibition ability of these clones is strong, modest, and poor, respectively. We next observed whether or not these antibodies inhibit human blood clotting. Antibody 1849 strongly inhibited fibrin clotting in a concentration-dependent manner and prolonged the clotting time to the same level as spontaneous clotting without TF. Antibody 72 modestly inhibited fibrin clotting. In contrast, antibody 130 was unable to inhibit fibrin clotting (Supplemental Fig. B). The same results were obtained using mouse plasma (Supplemental Fig. C). These results suggested that rat anti-human TF antibody purified from hybridoma clone 1849 possessed the most potent TF neutralising effect in terms of blood coagulation cascade. We also determined whether or not antibody 1849 inhibits the TF-VIIa-mediated cell signalling pathway. To determine if 1849 inhibits MMP-9, we examined MMP-9 production by gelatin zymography in BxPC3 mock in the presence of factor VIIa. It was observed that factor VIIa promoted MMP-9 production in BxPC3 mock again (Fig. 2B, Supplemental Fig. D). Interestingly, TF neutralisation antibody 1849 suppressed TF-VIIa-mediated MMP-9 production partly, but the non-specific antibody was unable to suppress production (Supplemental Fig. D). This result showed that antibody 1849 could inhibit not only fibrin clotting but also TF-related cell signalling. Immunocytochemistry with 1849 showed TF in TF-positive cells (Capan1 and BxPC3), whereas there was no detectable TF in TF-negative cells (Panc1 and Mia Paca2) (Supplemental Fig. E). In addition, we confirmed that human TF interacts with mouse factor VIIa, and 1849 inhibits the interaction of human TF and mouse factor VIIa (Supplemental Fig. C), but 1849 does not react with mouse TF (data not shown).

3.4. *Inhibitory effect of anti-TF mAb (1849) on cancer cell invasion in vitro*

Since 1849 was able to block both TF-related cell signalling and the blood coagulation function (Supplemental Figures), we predicted that it would inhibit both the promotion of cancer invasion via TF-related cell signalling and haematogenous metastasis via TF-related blood coagulation function. First, we examined the invasion ability in BxPC3 mock in the presence of factor VIIa and/or TF neutralisation antibody

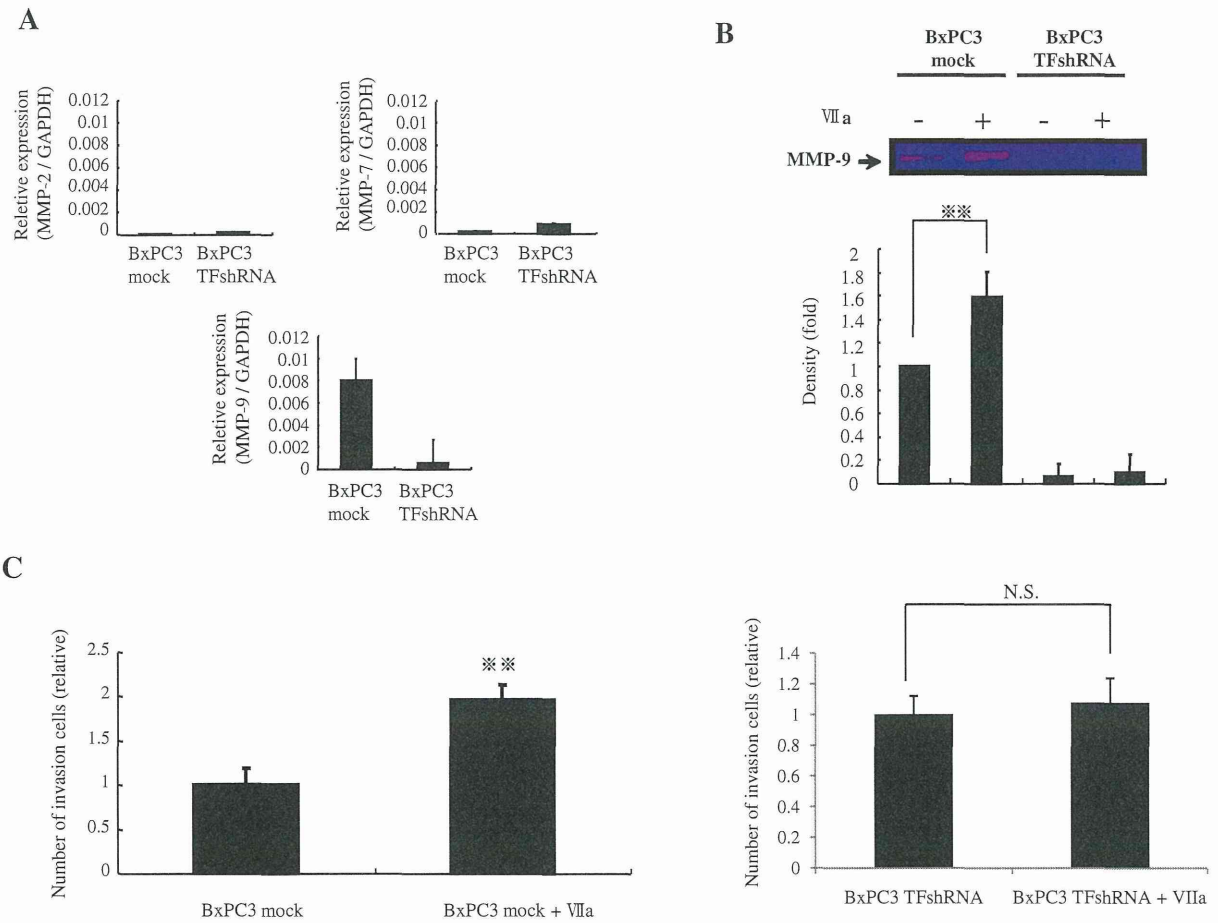

Fig. 2 – TF-VIIa complex promotes the expression of MMP-9 and invasion. (A) Expression of MMP-2, MMP-7 and MMP-9 by real-time PCR in BxPC3 mock and BxPC3 TFshRNA. Data are expressed as the mean ± SD. (B) Gelatin zymography of culture medium in BxPC3 mock and BxPC3 TFshRNA with or without factor VIIa (5 nM) after starvation for 2 h. MMP-9 was quantified using Image J software. Data are expressed as the mean ± SD. ** $P < 0.01$. (C) Invasion ability in BxPC3 mock or BxPC3 TFshRNA treated with factor VIIa (50 nM). Data are expressed as the mean ± SD. ** $P < 0.01$. N.S. means not significant.

1849. *In vitro* invasion study showed that the TF neutralisation antibody inhibited the invasion of BxPC3 mock in the presence of factor VIIa compared with the non-specific antibody (Fig. 3A).

3.5. *Effect of anti-TF mAb (1849) in mouse model*

In the portal-injection liver metastasis model, cancer cells stayed in the liver and luminescence continued to increase in a time-dependent manner in the control group. On the other hand, in the mice receiving 1849 treatment, luminescence began to decrease from 5 to 10 h after the injection of cancer cells (Fig. 3B). 1849 completely inhibited liver metastasis on Day 4, but the control did not (Fig. 3C). In the orthotopic pancreatic tumour xenograft model, remarkably strong invasion and metastasis were manifested in the liver, mesentery and stomach in the control group (Fig. 4A). In contrast, TF neutralisation antibody 1849 was able to suppress invasion (Fig. 4A). Furthermore, the progression score reflecting invasion and metastasis in the pancreatic orthotopic tumour xenograft was significantly lower in the 1849-treatment group compared with that in the control group (Fig. 4B). In addition, cancer spreading beyond the pancreas was observed in the control group. On the other hand, pancreatic cancer cells remained within the pancreas even after 6 weeks of injection of cancer cells in the 1849-treatment group (Fig. 4C). Kaplan–Meier analysis showed a significant improvement in survival rate in the 1849 treatment group compared to the control group (Fig. 4D). A significant difference in body change between the 1849-treatment mice and the control mice was not observed (Fig. 4E).

4. Discussion

Pancreatic cancer is the most refractory neoplasm and possesses several clinicopathological characteristics. First, pancreatic cancer exerts extensive invasion and metastasis to other organs.[14,15] Second, thrombosis occurs most frequently in patients with pancreatic cancer.[7] Third, expression of TF may contribute to the aggressiveness of pancreatic cancer that stimulates tumour invasiveness, and evaluation of the primary tumour for TF expression may identify patients with a poor prognosis.[17,18] We, therefore, hypothesised that TF

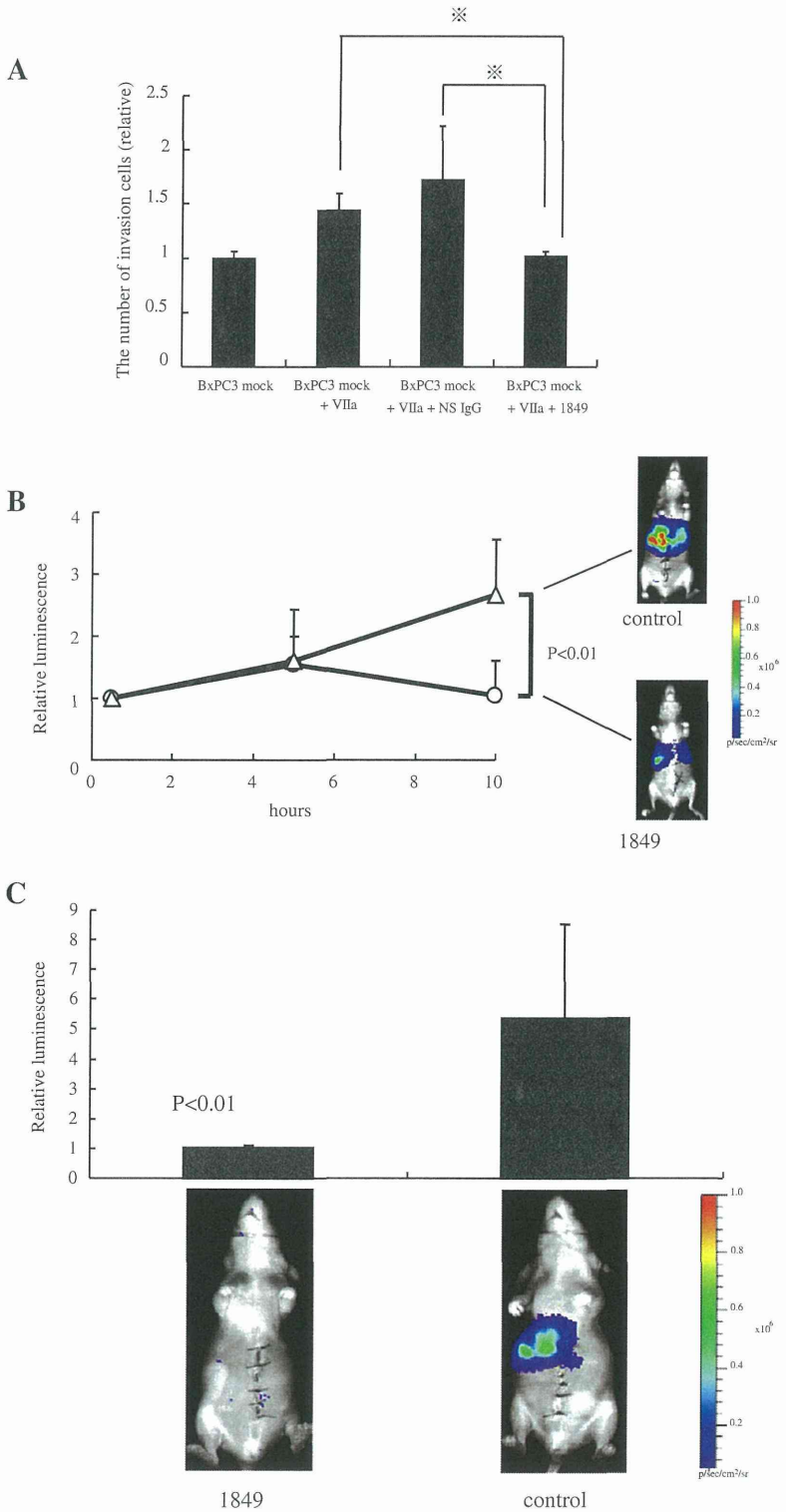

Fig. 3 – Anti-human neutralisation antibody 1849 inhibits cancer cell invasion and haematogenous metastasis. (A) Invasion ability in BxPC3 mock treated with factor VIIa (50 nM) clone 1849 (100 μg/ml), or non-specific antibody (anti-human CD20 antibody, 100 μg/ml). Data are expressed as the mean ± SD. * $P < 0.05$. (B) Inhibition of early-phase metastasis by 1849 in portal-injection liver metastasis model. Luminescence intensity was measured by IVIS imaging system 0, 5, and 10 h after injection of cancer cells. Data are expressed as the mean ± SD. $N = 6$. (C) Inhibition of late-phase metastasis by 1849. Luminescence intensity was measured by IVIS imaging system 4 days after injection of cancer cells. Data are expressed as the mean ± SD. $N = 5$.

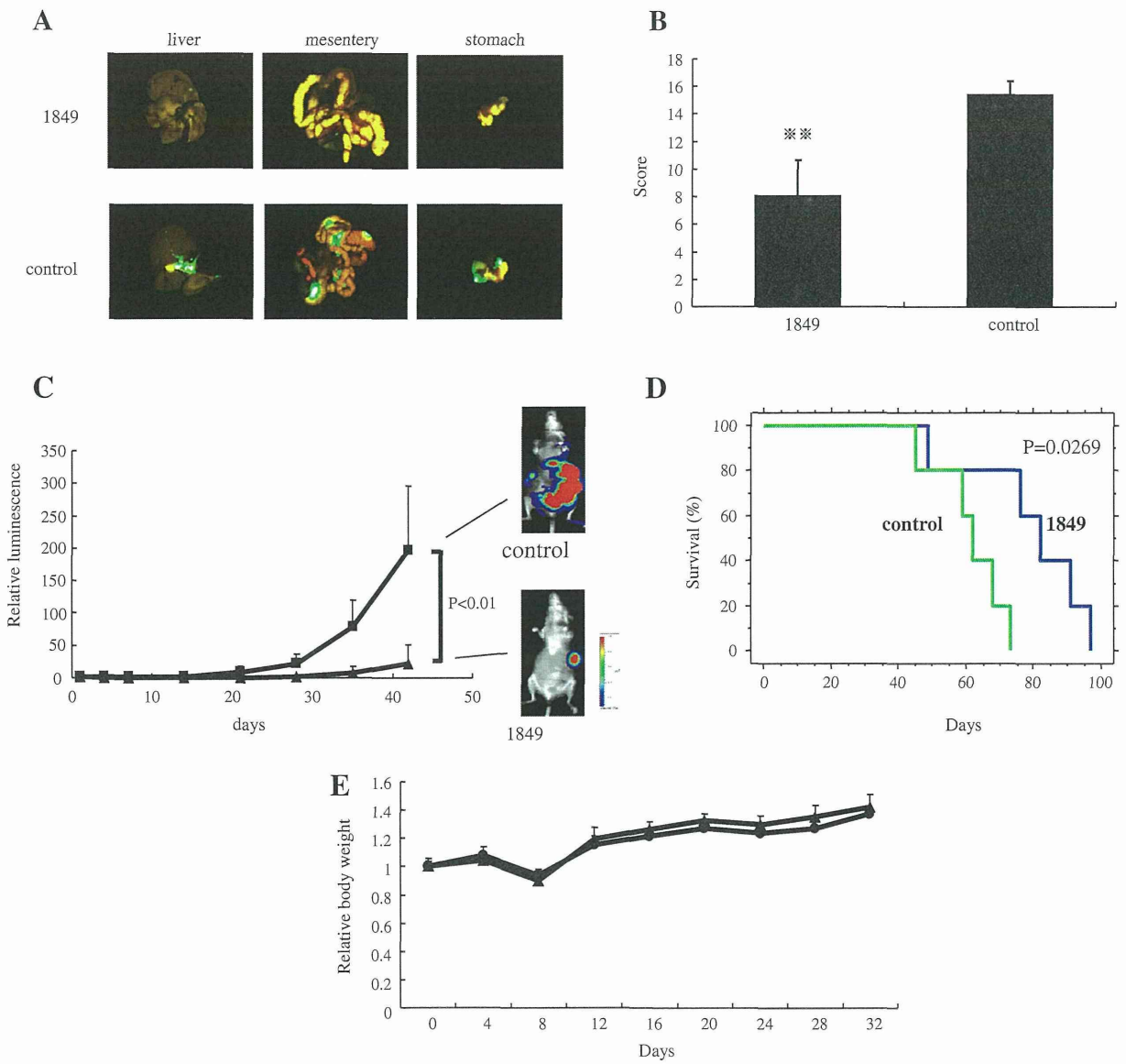

Fig. 4 – The effect of 1849 in the mouse model. (A) Representative fluorescence images of liver, mesentery and stomach bearing BxPC3 mock GFP treated with 1849 or PBS. GFP signal denotes the presence of tumour cells. (B) A dissemination score was calculated to evaluate local tumour invasion and distant metastasis as previously described. Data are expressed as the mean ± SD. $N = 5–6$. ** $P < 0.01$. (C) Inhibition of invasion and metastasis by 1849 in pancreatic orthotopic tumour xenografts. Relative luminescence was quantitated by IVIS imaging system. Representative luminescence intensity images were obtained in the individual control and the 1849-treated group. Data are expressed as the mean ± SD. $N = 5$. D. Effect of 1849 treatment on survival. Survival was assessed by Kaplan–Meier analysis. Blue line represents the 1849 treatment group. Green line indicates the control group. $N = 5$. E. Body weight change by 1849. Mice inoculated with BxPC3 cells subcutaneously on Day 0 were treated for seven consecutive days with 1849 mAb (400 μg/mouse, ●) as the TF neutralisation antibody, or PBS (▲) as the control. $N = 3$.

plays an important role in the invasion-metastasis cascade of pancreatic cancer.

In this study, the expression pattern of TF in BxPC3, TF-abundant cancer cells, was different between *in vitro* and *in vivo*. These results corresponded with a previous study on the human squamous cell carcinoma cell line A431.[21] Both A431 and BxPC3 are uniformly expressed *in vitro*. A431 xenografts were heterogeneously stained for TF; however, our study showed BxPC3 xenografts highly expressed in the area of cancer cells contacting with stromal cells, namely the invasion front. In fact, invasion assay showed that BxPC3 TFshRNA cell lines strongly inhibited cell invasion compared with BxPC3 mock cell lines. Real-time PCR analysis showed that the expression of MMP-9 in the BxPC3 TFshRNA cell line decreased compared with BxPC3 mock. To date, many reports have shown that MMP-9 promotes the invasion of pancreatic cancer.[3,22] In BxPC3, the invasion ability was suppressed through the inhibition of MMP-9 expression by SiRNA.[23]

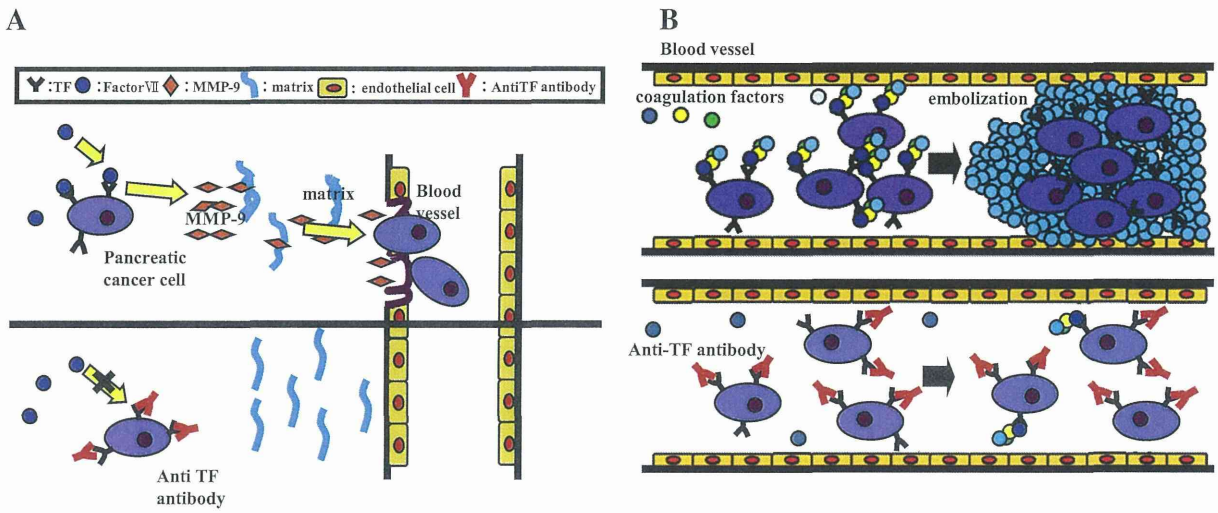

Fig. 5 – Possible role of TF-VIIa complex on invasion and metastasis. And the implication of anti-human TF neutralisation antibody, 1849, against the tumour metastasis. (A) TF-VIIa in pancreatic cancer induces MMP-9 expression and invades stromal tissue and basement membrane. 1849 inhibits invasion by inhibiting TF-related cell signalling. (B) TF-VIIa promotes embolisation in micro blood vessels. 1849 inhibits blood coagulation and traps cancer cells.

Taking our present data and other reports together, TF promotes the invasion ability of BxPC3 by expressing MMP-9.

Previous reports showed the relationship between coagulation factors and MMPs. In normal tissue, PAR-2, which is downstream from TF-VIIa complex signalling, mediates MMP-9 release in airway epithelial cells.[24] Thrombin mediates an increase in MMP-1 and MMP-3 in human endothelial cells.[25] In cancer tissue, PARs mediate MMP-2 and MMP-9 in prostate cancer.[26] Also, in colorectal adenocarcinoma cells, the TF-VIIa complex induces the expression of MMP-7.[27] However, in pancreatic cancer cells, the relationship between coagulation factor(s) and MMP(s) remains unclear. Our study is the first evidence that the TF-VIIa complex induces MMP-9 and promotes invasion in pancreatic cancer cells. Moreover, we also showed that TF promoted invasion *in vivo* using pancreatic orthotopic tumour xenografts.

Next, we newly established a TF neutralisation antibody for the treatment of pancreatic cancer. We found that the anti-TF antibody 1849 decreased the release of MMP-9. Therefore, we propose that 1849 inhibits TF-related cell signalling by blocking the TF-VIIa complex. Also, blood coagulation assay showed that 1849 inhibited TF-induced blood coagulation to the same level as the TF-free sample. We suggest from this result that 1849 can almost completely inhibit TF-related blood coagulation.

We found that 1849 inhibited pancreatic cancer invasion in the *in vitro* invasion assay. We suggest that this anti-invasion effect of 1849 is due to MMP-9 suppression via TF-related cell signalling. Also, 1849 completely blocked haematogenous metastasis in the portal-injection liver metastasis mouse model. This result suggested that the anti-haematogenous metastasis effect of 1849 is due to blocking the TF-related blood coagulation cascade.

Since the metastatic ability of BxPC3 TFshRNA decreased significantly as compared to that of BxPC3 mock *in vivo*, we tested if our newly developed anti- TF mAb suppressed the metastasis of BxPC3. We used the orthotopic pancreatic tumour xenograft model to examine whether or not 1849 could block invasion and metastasis in the mouse model, because the orthotopic model is similar to human pancreatic cancer in terms of progression, invasion, and metastasis.[19] 1849 strongly inhibited invasion and metastasis. Moreover, the survival rate in the 1849 treatment group was significantly improved compared with that of the control group.

The metastasis process includes many steps. Cancer cells invade the basement membrane and the pericytes of blood vessels. Cancer cells survive in the bloodstream and end up in the micro blood vessels of distant organs. MMP-9 plays an important role in invasion. Fibrin facilitates metastasis by enhancing the sustained adherence and survival of tumour cell emboli in the blood vessels of distant organs.[10] Also, a recent study showed that fibrin increases the metastatic potential of circulating tumour cells by impeding natural killer cells.[28] 1849 almost completely inhibited both blood coagulation and TF-VIIa complex mediated MMP-9 release.

In summary, we found that the TF-VIIa complex upregulated MMP-9 and promoted cancer invasion in pancreatic cancer. The cancer cells subsequently degraded the stromal extracellular matrix and basement membrane to intravasate into the blood vessels (Fig. 5A). Next, they formed microthrombi within the vessels (Fig. 5B). The double-blocking effect of our newly developed TF neutralisation antibody 1849 could be a useful tool in the treatment of pancreatic cancer invasion-metastasis.

Grant support

This work was supported partly by a Grant-in-Aid from the Third Term Comprehensive Control Research for Cancer, the Ministry of Health, Labor and Welfare (Matsumura, H19-025), Scientific Research on Priority Areas from the Ministry of Education, Culture, Sports, Science and Technology

(Matsumura, 17016087), and the Japanese Foundation for Multidisciplinary Treatment of Cancer (Matsumura), Funding Program for World-Leading Innovative R&D on Science and Technology (FIRST Program) and the Princess Takamatsu Cancer Research Fund (07-23908). Yohei Saito was supported by Research Fellowships from the Japan Society for the Promotion of Science for Young Scientists.

Conflict of interest statement

None declared.

Acknowledgements

We thank Dr. Miyawaki (RIKEN) for Venus. We thank N. Mie and M. Ohtsu for their technical assistance, and K. Shiina for her secretarial assistance.

Appendix A. Supplementary data

Supplementary data associated with this article can be found, in the online version, at doi:10.1016/j.ejca.2011.04.028.

REFERENCES

1. Fidler IJ. The pathogenesis of cancer metastasis: the 'seed and soil' hypothesis revisited. *Nat Rev Cancer* 2003;**3**:453–8.
2. Curran S, Murray GI. Matrix metalloproteinases: molecular aspects of their roles in tumour invasion and metastasis. *Eur J Cancer* 2000;**36**:1621–30.
3. Nagakawa Y, Aoki T, Kasuya K, Tsuchida A, Koyanagi Y. Histologic features of venous invasion, expression of vascular endothelial growth factor and matrix metalloproteinase-2 and matrix metalloproteinase-9, and the relation with liver metastasis in pancreatic cancer. *Pancreas* 2002;**24**:169–78.
4. Edgington TS, Mackman N, Brand K, Ruf W. The structural biology of expression and function of tissue factor. *Thromb Haemost* 1991;**66**:67–79.
5. Ruf W, Edgington TS. Structural biology of tissue factor, the initiator of thrombogenesis *in vivo*. *FASEB J* 1994;**8**:385–90.
6. Varki A. Trousseau's syndrome: multiple definitions and multiple mechanisms. *Blood* 2007;**110**:1723–9.
7. Stein PD, Beemath A, Meyers FA, et al. Incidence of venous thromboembolism in patients hospitalized with cancer. *Am J Med* 2006;**119**:60–8.
8. Belting M, Ahamed J, Ruf W. Signaling of the tissue factor coagulation pathway in angiogenesis and cancer. *Arterioscler Thromb Vasc Biol* 2005;**25**:1545–50.
9. Sampson MT, Kakkar AK. Coagulation proteases and human cancer. *Biochem Soc Trans* 2002;**30**:201–7.
10. Palumbo JS, Kombrinck KW, Drew AF, et al. Fibrinogen is an important determinant of the metastatic potential of circulating tumor cells. *Blood* 2000;**96**:3302–9.
11. Morris DR, Ding Y, Ricks TK, et al. Protease-activated receptor-2 is essential for factor VIIa and Xa-induced signaling, migration, and invasion of breast cancer cells. *Cancer Res* 2006;**66**:307–14.
12. Hjortoe GM, Petersen LC, Albrektsen T, et al. Tissue factor-factor VIIa-specific up-regulation of IL-8 expression in MDA-MB-231 cells is mediated by PAR-2 and results in increased cell migration. *Blood* 2004;**103**:3029–37.
13. Jemal A, Siegel R, Ward E, et al. Cancer statistics, 2008. *CA Cancer J Clin* 2008;**58**:71–96.
14. Warshaw AL, Fernández-del Castillo C. Pancreatic carcinoma. *N Engl J Med* 1992;**326**:455–65.
15. Wanebo HJ, Vezeridis MP. Pancreatic carcinoma in perspective. A continuing challenge. *Cancer* 1996;**78**:580–91.
16. Khorana AA, Ahrendt SA, Ryan CK, et al. Tissue factor expression, angiogenesis, and thrombosis in pancreatic cancer. *Clin Cancer Res* 2007;**13**:2870–5.
17. Kakkar AK, Lemoine NR, Scully MF, Tebbutt S, Williamson RC. Tissue factor expression correlates with histological grade in human pancreatic cancer. *Br J Surg* 1995;**82**:1101–4.
18. Nitori N, Ino Y, Nakanishi Y, et al. Prognostic significance of tissue factor in pancreatic ductal adenocarcinoma. *Clin Cancer Res* 2005;**11**:2531–9.
19. Saito Y, Yasunaga M, Kuroda J, Koga Y, Matsumura Y. Antitumour activity of NK012, SN-38-incorporating polymeric micelles, in hypovascular orthotopic pancreatic tumour. *Eur J Cancer* 2010;**46**:650–8.
20. Hotz HG, Reber HA, Hotz B, et al. An orthotopic nude mouse model for evaluating pathophysiology and therapy of pancreatic cancer. *Pancreas* 2003;**26**:e89–98.
21. Milsom CC, Yu JL, Mackman N, et al. Tissue factor regulation by epidermal growth factor receptor and epithelial-to-mesenchymal transitions: effect on tumor initiation and angiogenesis. *Cancer Res* 2008;**68**:10068–76.
22. Määttä M, Soini Y, Liakka A, Autio-Harmainen H. Differential expression of matrix metalloproteinase (MMP)-2, MMP-9, and membrane type 1-MMP in hepatocellular and pancreatic adenocarcinoma: implications for tumor progression and clinical prognosis. *Clin Cancer Res* 2000;**6**:2726–34.
23. Wang Z, Banerjee S, Li Y, et al. Down-regulation of notch-1 inhibits invasion by inactivation of nuclear factor-kappaB, vascular endothelial growth factor, and matrix metalloproteinase-9 in pancreatic cancer cells. *Cancer Res* 2006;**66**:2778–84.
24. Vliagoftis H, Schwingshackl A, Milne CD, et al. Proteinase-activated receptor-2-mediated matrix metalloproteinase-9 release from airway epithelial cells. *J Allergy Clin Immunol* 2000;**106**:537–45.
25. Duhamel-Clérin E, Orvain C, Lanza F, Cazenave JP, Klein-Soyer C. Thrombin receptor-mediated increase of two matrix metalloproteinases, MMP-1 and MMP-3, in human endothelial cells. *Arterioscler Thromb Vasc Biol* 1997;**17**:1931–8.
26. Wilson SR, Gallagher S, Warpeha K, Hawthorne SJ. Amplification of MMP-2 and MMP-9 production by prostate cancer cell lines via activation of protease-activated receptors. *Prostate* 2004;**60**:168–74.
27. Zhang JQ, Wan YL, Liu YC, et al. The FVIIa-tissue factor complex induces the expression of MMP7 in LOVO cells *in vitro*. *Int J Colorectal Dis* 2008;**23**:971–8.
28. Palumbo JS, Talmage KE, Massari JV, et al. Platelets and fibrin(ogen) increase metastatic potential by impeding natural killer cell-mediated elimination of tumor cells. *Blood* 2005;**105**:178–85.

ARTICLE IN PRESS
COREL-06196; No of Pages 8
Journal of Controlled Release xxx (2012) xxx–xxx
Contents lists available at SciVerse ScienceDirect
Journal of Controlled Release
journal homepage: www.elsevier.com/locate/jconrel

Polymeric micelles incorporating (1,2-diaminocyclohexane)platinum (II) suppress the growth of orthotopic scirrhous gastric tumors and their lymph node metastasis

Md. Rafi [a], H. Cabral [b], M.R. Kano [c,f], P. Mi [b], C. Iwata [c], M. Yashiro [d], K. Hirakawa [d], K. Miyazono [c,f], N. Nishiyama [a,f,*], K. Kataoka [a,b,e,f,**]

[a] Center for Disease Biology and Integrative Medicine, Graduate School of Medicine, The University of Tokyo, 7-3-1 Hongo, Bunkyo-ku, Tokyo 113-0033, Japan
[b] Department of Bioengineering, Graduate School of Engineering, The University of Tokyo, 7-3-1 Hongo, Bunkyo-ku, Tokyo, 113-8656, Japan
[c] Department of Molecular Pathology, Graduate School of Medicine, The University of Tokyo, 7-3-1 Hongo, Bunkyo-ku, Tokyo 113-0033, Japan.
[d] Department of Surgical Oncology, Medical School, Osaka City University, Osaka, Japan
[e] Department of Materials Engineering, Graduate School of Engineering, The University of Tokyo, 7-3-1 Hongo, Bunkyo-ku, Tokyo 113-8656, Japan
[f] Center for NanoBio Integration, The University of Tokyo, 7-3-1 Hongo, Bunkyo-ku, Tokyo 113-8656, Japan

ARTICLE INFO

Article history:
Received 24 October 2011
Accepted 27 January 2012
Available online xxxx

Keywords:
Drug delivery
Chemotherapy
Polymeric micelles
Gastric cancer
Lymph node metastasis

ABSTRACT

Nano-scaled drug carriers have great potential for the treatment of solid tumors. Nevertheless, hypovascularity and fibrosis in some types of solid tumors have been demonstrated to reduce the penetration and accumulation of nano-scaled drug carriers. Diffuse-type scirrhous gastric cancers present such characteristics as well as frequent metastasis to the lymph nodes; therefore, it remains a great challenge to eradicate scirrhous gastric cancers based on the drug targeting using nanocarriers. Herein, we demonstrated that polymeric micelles with 30-nm diameter incorporating (1,2-diaminocyclohexane)platinum(II) (DACHPt), the parent complex of the anticancer drug oxaliplatin, efficiently penetrated and accumulated in an orthotopic scirrhous gastric cancer model, leading to the inhibition of the tumor growth. Moreover, the elevated localization of systemically injected DACHPt-loaded micelles in metastastic lymph nodes reduced the metastatic tumor growth. These results suggest DACHPt-loaded micelles as a promising nanocarrier for the treatment of scirrhous gastric cancers and their lymphatic metastases.

1. Introduction

Nano-scaled drug carriers are being developed for improving the treatment of solid tumors while decreasing the toxicity [1–5]. These nanocarriers effectively accumulate in solid tumors due to the hyperpermeability of blood capillaries to circulating macromolecules and the impaired lymphatic drainage of these macromolecules, which are known as the Enhanced Permeability and Retention (EPR) effect [6]. Indeed, several nanocarrier formulations have been approved for clinical use against hypervascular cancers such as ovarian cancers, HIV-associated Kaposi's sarcoma and breast cancers [7,8]. However, in some intractable cancers such as pancreatic and gastric cancers, the hypovascularity and fibrosis of tumors may compromise the extravasation and tissue penetration of nanocarriers [9,10].

Gastric cancers cause 1 million deaths per year worldwide being the 2nd leading cause of cancer-related death following lung cancer [11]. Among gastric cancers, a diffuse-type scirrhous gastric cancer (SGC) affects younger patients and presents the highest mortality [12]. SGC is characterized by hypovascularity, extensive stromal fibrosis and metastasis to the lymph nodes [13–15]. These characteristics impair the therapeutic efficacy of chemotherapy as well as nanocarrier-mediated targeting chemotherapy. Moreover, the targeting chemotherapy against lymph node metastasis involve intralymphatic or local administration of nanocarrier-encapsulated antitumor agents [16–18]; however, these approaches may not target all draining lymph nodes due to the inappropriate position of the injection [18] and the obstruction of lymphatic vessels in advanced stages of cancer [18–19]. Hence, the improved targeting against the lymph node metastasis is strongly needed to eradicate the lymph node metastasis.

Polymeric micelles, self-assemblies of block copolymers are characterized by the core-shell structures with drug-loaded core surrounded by hydrophilic PEG shell, and have shown great potential as tumor-targetable nanocarriers [3–5]. The substantial advantages of polymeric micelles include relatively small size ranging from 20 to 100 nm, controllable drug loading and release, and favorable biodistribution including prolonged blood circulation and enhanced tumor accumulation [3–5]. Accordingly, micelle formulations

* Correspondence to: N. Nishiyama, Center for Disease Biology and Integrative Medicine, Graduate School of Medicine, The University of Tokyo, 7-3-1 Hongo, Bunkyo-ku, Tokyo 113-0033, Japan. Tel.: +81 3 5841 1430; fax: +81 3 5841 1419.
** Correspondence to: K. Kataoka, Department of Materials Engineering, Graduate School of Engineering, The University of Tokyo, 7-3-1 Hongo, Bunkyo-ku, Tokyo 113-8656, Japan. Tel.: +81 3 5841 7138; fax: +81 3 5841 7139.
E-mail addresses: nishiyama@bmw.t.u-tokyo.ac.jp (N. Nishiyama), kataoka@bmw.t.u-tokyo.ac.jp (K. Kataoka).

0168-3659/$ – see front matter © 2012 Elsevier B.V. All rights reserved.
doi:10.1016/j.jconrel.2012.01.038

incorporating doxorubicin, SN-38, paclitaxel, cisplatin, and (1,2-diaminocyclohexane)platinum(II) (DACHPt) (an active form of oxaliplatin) exerted significant efficacy against several tumor models with appreciably lowered toxicity compared to free drugs, and are currently under clinical evaluation [20–24]. Particularly, DACHPt-loaded polymeric micelles (DACHPt/m) are characterized by the small size (ca. 30 nm) [25–26], achieving high penetration into tumor mass and remarkable antitumor activity against poorly permeable tumors such as pancreatic tumors [27–29].

This study was aimed to evaluate the targeting ability and therapeutic efficiency of systemically injected DACHPt/m against a well-established experimental model of SGC, which was prepared by orthotopic inoculation of OCUM-2MLN scirrhous gastric cancer cells [30–31]. In the orthotopic SGC model of OCUM-2MLN cells, the induction of lymph node metastasis occurs in all mice, while the tumor microenvironment shows hypovascularity and thick fibrosis similar to SGC in the patients, indicating the clinical relevancy of this model [30–31]. Here, the therapeutic potential of the DACHPt/m against orthotopic SGC and their lymph node metastasis was examined by using bioluminescent OCUM-2MLN-Luc tumors.

2. Materials and methods

2.1. Materials

Bis(trichloromethyl)carbonate (triphosgene) was purchased from Tokyo Kasei Kogyo Co., Inc. (Tokyo, Japan). γ-Benzyl L-glutamate was purchased from Sigma Chemical Co., Inc. (St. Louis, MO). *N,N*-Dimethylformamide (DMF) and 3-(4,5-dimethylthiazol-2-yl)-2,5-diphenyltetrazolium bromide (MTT) were obtained from Wako Pure Chemical Co., Inc. (Osaka, Japan). Dichloro(1,2-diamminocyclohexane) platinum(II) ($DACHPtCl_2$) was purchased from Heraeus (Germany). $AgNO_3$ was purchased from Aldrich Chemical Co., Inc. (Milwaukee, WI). α-Methoxy-ω-amino poly(ethylene glycol) (CH_3O-PEG-NH_2; Mw = 12,000) was purchased from NOF Co., Inc. (Tokyo, Japan). Alexa 594- and Alexa 680-*N*-hydroxysuccinimide ester were purchased from Invitrogen (USA).

2.2. Animals and cells

Immunodeficient BALB/c nu/nu mice at 6 weeks of age were obtained from Charles River Laboratories (Tokyo, Japan), and treated in accordance with the policies of the Animal Ethics Committee of The University of Tokyo. Human diffuse-type gastric carcinoma OCUM-2MLN cells were used for the model of diffuse-type scirrhous gastric cancer (SGC) with high frequency of the lymph node metastasis [30–31]. OCUM-2MLN cells were maintained in Dulbecco's Modified Eagle Media (DMEM) (Sigma Chemicals) supplemented with 10% fetal bovine serum (FBS) in a humidified atmosphere containing 5% CO_2 at 37 °C.

2.3. Preparation of PEG-b-P(Glu)

Poly(ethylene glycol)-poly(L-glutamic acid) block copolymers (PEG-*b*-P(Glu)) were synthesized according to the previously described synthetic method with a slight modification [25]. Briefly, *N*-carboxy anhydride of γ-benzyl L-glutamate was polymerized in DMF, initiated by the primary amino group of CH_3O-PEG-NH_2 to obtain PEG-poly(γ-benzyl-L-glutamate) block copolymer (PEG-*b*-PBLG). A narrow distribution (Mw/Mn: 1.06) of PEG-*b*-PBLG was confirmed by gel permeation chromatography [column: TSK-gel G3000HHR, G4000HHR (Tosoh, Yamaguchi, Japan); eluent: DMF containing 10 mM LiCl; flow rate: 0.8 ml/min; detector: refractive index (RI); temperature: 25 °C]. The polymerization degree of PBLG was determined to be 20 by comparing the proton ratios of methylene units in PEG (—OCH_2CH_2—: δ = 3.7 ppm) and phenyl groups of PBLG (—$CH_2C_6H_5$—: δ = 7.3 ppm) in ^{1}H-NMR measurement [JEOL EX270 (JEOL, Tokyo, Japan); solvent: DMSO-d_6; temperature: 80 °C]. The deprotection of the benzyl group of PEG-*b*-PBLG was carried out by mixing with 0.5 N NaOH at room temperature to obtain PEG-*b*-P(Glu).

PEG-*b*-P(Glu) was fluorescent-labeled by the conjugation of Alexa 594- or Alexa 680-succinimidyl esters to the ω-amino group of the polymer in DMSO. Twenty-four hours later, the polymers were purified by dialysis against DMSO followed by water. Finally, the solutions were freeze-dried, and the amount of conjugated dye was determined to be approximately 70% (% fluorescent dye / PEG-*b*-P(Glu)) by fluorescence spectroscopy.

2.4. Preparation of DACHPt-loaded micelles (DACHPt/m)

DACHPt/m were prepared according to a previously described method [25]. Briefly, $DACHPtCl_2$ (5 mM) was suspended in distilled water and mixed with silver nitrate [($AgNO_3$)/(DACHPt) = 1] to form DACHPtCl(NO_3). The solution was kept in the dark for 24 h at 25 °C. AgCl precipitate after reaction was eliminated by centrifugation. The supernatant was purified by passage through a 0.22 μm filter. Then, PEG-*b*-P(Glu) [(Glu) = 5 mmol/l] was added to the DACHPt solution [(DACHPt)/(Glu) = 1.0] and reacted for 120 h to prepare DACHPt/m. The prepared micelles were purified by ultrafiltration [molecular weight cutoff size (MWCO): 30,000]. The size distribution of DACHPt/m was evaluated by dynamic light scattering (DLS) measurement at 25 °C, using the Zetasizer Nano ZS90 (Malvern Instruments Ltd., Worcestershire, United Kingdom).

The Pt content of the micelles was determined by using an ion coupled plasma-mass spectrometer (4500 ICP-MS; Hewlett Packard, Palo Alto, CA). Fluorescent-labeled DACHPt/m were prepared in a similar manner with Alexa 594- or Alexa 680-labeled PEG-P(Glu).

2.4.1. In vitro cytotoxicity assay

To determine the cytotoxicity, OCUM-2MLN cells were seeded in a 96 well plate and incubated at 37 °C. Then, the cells were exposed to free oxaliplatin or DACHPt/m for 48 or 72 h, followed by the addition of MTT solution. Cell viability was measured by the formed formazan absorbance at 570 nm.

2.5. Preparation of orthotopic SGC models with lymphatic metastasis

Lentiviral vector [32] was used to express the luciferase protein gene stably in OCUM-2MLN cells. The prepared OCUM-2MLN-Luc cells were grown in DMEM containing 10% FBS. For preparation of orthotopic SGC models, OCUM-2MLN-Luc cells were inoculated by orthotopic implantation method. Briefly, after the abdomen of BALB/c nu/nu mice was sterilized with alcohol, an incision was made to expose the stomach, and OCUM-2MLN-Luc cell suspension was injected sub-serosally into the gastric walls as previously described [33]. The stomach was then returned into the peritoneal cavity, and the abdominal wall and the skin were closed with surgical suture.

2.6. Evaluation of antitumor activity by bioluminescent imaging

Bioluminescent imaging [34] was carried out with a highly sensitive CCD camera using IVIS imaging system (IVIS, Caliper Life Science, Hopkinton, MA). Imaging and quantification of signals were analyzed by Living Image software (Caliper Life Science). For *in vitro* imaging, bioluminescent cells were diluted in cell culture media in a black, 96-well plate (Costar, Corning, NY). VivoGlo luciferin (Promega, Madison, WI) at 150 μg/ml in media was added to each well 5 min prior to imaging. Imaging was performed for 1 min per plate. For the analysis of antitumor activity, BALB/c nu/nu ($n = 5$) mice were inoculated by orthotopic injection of OCUM-2MLN –Luc cells (5×10^6). Tumors were allowed to grow for 3 weeks, to initiate the metastasis to the lymph nodes. Subsequently, the mice received three i.v. injections of oxaliplatin (8 mg/kg)

Please cite this article as: M. Rafi, et al., Polymeric micelles incorporating (1,2-diaminocyclohexane)platinum (II) suppress the growth of orthotopic scirrhous gastric tumors ..., J. Control. Release (2012), doi:10.1016/j.jconrel.2012.01.038